Waveguide Integrated Photodiode for Analog Fiber-Optics Links

Hao Jiang and Paul K. L. Yu, *Senior Member, IEEE*

***Abstract*—We present the design, fabrication, and characterization of a vertically coupled 1.3-μm wavelength waveguide integrated InGaAs photodiode with distributed absorption. This design, by employing an index-matching layer and a thick waveguiding layer, can yield a significant improvement in the optical power saturation, responsivity, and speed in the same device. The 1-dB compression point of the photodiode response at 20 GHz occurs at 10.2-mA continuous-wave photocurrent. Moreover, the same device exhibits a 47-GHz 3-dB bandwidth with a 50-Ω microwave probe, and a 0.4-A/W microwave responsivity at 20 GHz without antireflection coating at the input facet. Its two-tone output referenced third-order intercept point is $+20.32$ dBm at 1 GHz and $+5.25$ dBm at 18 GHz.**

***Index Terms*—Analog systems, optical saturation, photodiodes, waveguides.**

I. Introduction

FOR AN externally modulated analog fiber-optics link, the radio-frequency (RF) link gain and the noise figure can be improved by using high-power low relative-intensity-noise optical source or a low-noise optical amplifier, provided that the photodiode at the receiver has a high responsivity and does not saturate at high optical power [1]. For the same link, the spurious-free dynamic range (SFDR) can be enhanced at high power provided that the nonlinear distortions at the photodiode remain small [2]. For these reasons, it is essential to develop high-power photodiodes with high responsivity and high-speed properties for state-of-the-art analog fiber-optic links [3].

It has been shown that the optical saturation in photodiodes is caused by the space charge screening effect due to the dense photo-generated carriers [4], [5]. For side-illuminated waveguide photodiodes (WPs), the distribution of photo-generated carriers usually follows an exponential decay profile, with the highest absorption occurs at the front end. One approach to enhance the optical saturation level in these photodiodes is to use a diluted waveguide with a small modal confinement at the absorption layer to reduce the front-end absorption [6]. However, to keep the responsivity the same as that in ordinary lumped element waveguide photodiode [7], the diluted waveguide approach inevitably increases the length of the absorption waveguide (and thus a larger RC time and a lower speed). One way to overcome the RC time effect in a diluted waveguide photodiode (DWP) is to use the velocity-matched traveling-wave electrode [8].

Manuscript received March 2, 2000; revised September 14, 2000. This work was sponsored in part by TRW and in part by Photera Corporation.

The authors are with the Department of Electrical and Computer Engineering, University of California, San Diego, La Jolla, CA 92093-0407 USA.

Publisher Item Identifier S 0018-9480(00)10735-5.

The distributed absorption approach was proposed to ease the tradeoff between the speed and the power in the lumped element waveguide photodiode [9]. The distributed absorption arises from a gradual increase of the optical confinement factor $\Gamma(z)$ along the absorption waveguide, which in principle can lead to a more evenly distributed photocurrent profile favorable for high-power operation. However, in practice, very long absorption length (a few hundred micrometers) is required to achieve the distributed absorption in the horizontally coupled waveguide photodiode [9] and, as in the DWP case, the bandwidth of the photodiode is compromised.

In this paper, a waveguide integrated photodiode (WIP) with an index-matching layer, as shown in Fig. 1, is designed and fabricated for high-performance externally modulated analog links. When compared to similar photodiode designs recently proposed for high-speed operation [10]–[14], our WIP design can achieve high saturation current, responsivity, and speed together. Unlike the evanescent-coupled design proposed in [10], where the Γ of the absorber is constant [12], the corresponding $\Gamma(z)$ in our design varies periodically along the waveguiding direction. With the index-matching layer that ensures a high coupling efficiency between the passive waveguide and the absorber, effective distributed absorption can be achieved within a relatively short propagation distance via multimode beating induced by this layer. Also, the WIP can have a small Γ factor even with a relatively thick absorber since light is not directly coupled into the absorber in the WIP structure. The large absorption volume implies a lower current density, which is beneficial for high-power operation. Thus the photodiode is capable of delivering large photocurrent at high speed. Also, in contrast to the slab waveguide structure proposed in [11], where a thin ($\sim$0.6 μm) passive waveguide layer is employed, our design uses a ridge waveguide structure with a relatively thick passive waveguide layer ($\sim$1.2 μm), as shown in Fig. 1(b). This passive waveguide design allows a high coupling efficiency between the input fiber and the passive waveguide. The details of the WIP operation, the optical waveguide, and material designs with respect to device performance are given in Sections II and III; the fabrication of the WIP is summarized in Section IV; and Section V gives the measurement results of the WIP.

II. Operation of the WIPs

In a typical WIP operation, light is first coupled to a nonabsorbing passive waveguide that is connected to an absorber section where photocurrent is generated. The main design feature is the way to achieve an efficient optical coupling between

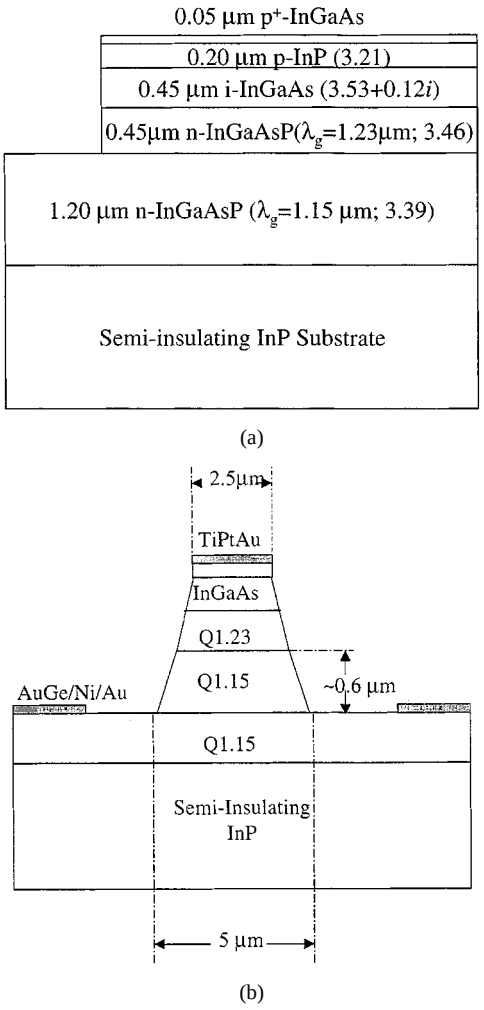

Fig. 1. (a) The material structure of the WIP. The intrinsic InGaAs is the absorber layer, the upper n-InGaAsP layer is the index-matching layer, and the lower one is the passive waveguiding layer. The bracket contains the layer bandgap and index at 1.3-μm wavelength. (b) Cross-sectional view of the absorber section of the WIP; the ridge includes 0.6 μm of the passive waveguide layer.

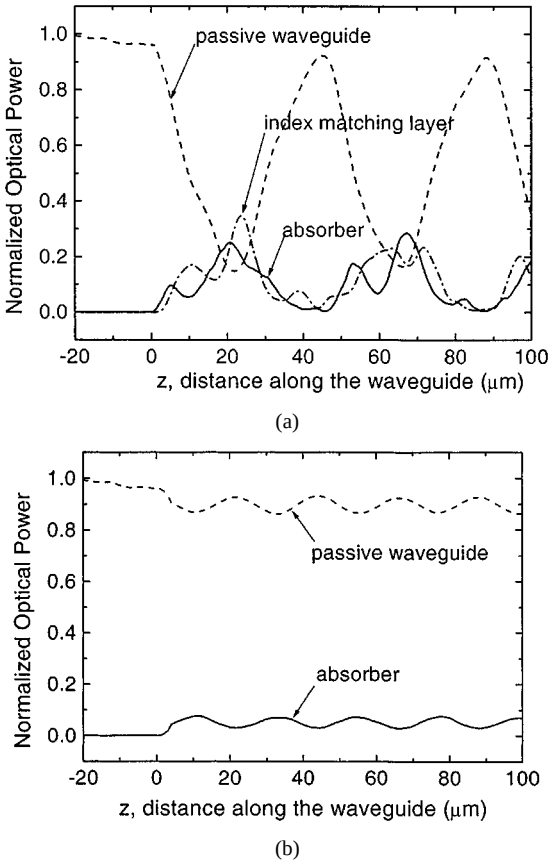

Fig. 2. (a) Normalized optical intensity distribution in the passive waveguide (dash line), the index-matching layer (dot line), and the absorber (solid line) for the structure shown in Fig. 1(a). The $z = 0$ point designates the beginning of the absorber. (b) Normalized optical intensity distribution in the passive waveguide (dash line) and the absorber (solid line) for the structure in Fig. 1(a) without the index-matching layer. The $z = 0$ point designates the beginning of the absorber.

the passive waveguide and the absorber. Deri *et al.* [14] demonstrated that the insertion of an index-matching layer between the passive waveguide and the absorber in a slab waveguide structure can enhance the coupling efficiency. The absorber length can be reduced from >100 μm to several tens of micrometers, which in turn improves the bandwidth of the lumped element photodiode.

In this paper, we further improve the design of WIP for high-power operation. The short absorber length and the resulting distributed absorption are both attributed to the inclusion of the index-matching layer. The material structure of the WIP is shown in Fig. 1(a), where 1.3 μm wavelength light is first coupled into the InGaAsP ($\lambda_g = 1.15$ μm) passive ridge waveguide. As the guided light reaches the section that incorporates the InGaAs absorber and the InGaAsP ($\lambda_g = 1.23$ μm) index matching layers, it is coupled into several transverse modes of the large optical waveguide. The beating of these modes causes the optical intensity distribution to oscillate between the passive waveguide and the absorber regions along the light propagation direction. As a result, the optical intensity can be transferred into the InGaAs absorber in a relatively short distance. A three-dimensional beam propagation method (BPM) simulator[1] is used to calculate the optical intensity distribution for the WIP depicted in Fig. 1, with and without the index-matching layer. In the simulation, a trapezoidal cross-section of the waveguide, as shown in Fig. 1(b), is assumed to represent the actual mesa shape of the device fabricated. Likewise, the width of the top p^+ InGaAs is set at 2.5 μm, and the width at the bottom of the etched mesa is 5 μm; the junction width is taken to be 3 μm as the intrinsic region is closer to the top. The optical indexes listed in Fig. 1(a) are for 1.32 μm wavelength. For the purpose of differentiating the coupling effect due to the index-matching layer, we initially set the absorptivity of the InGaAs to zero in the BPM simulation. The corresponding optical intensity in the InGaAs and the passive waveguide regions is plotted in Fig. 2(a). The simulation result suggests that along the waveguide $\sim$27% of the optical intensity in the original passive waveguide is periodically coupled to the InGaAs layer. The rest is distributed between the index-matching layer and the InP substrate. The vertical coupling behavior is caused by the optical mode beating [13] and is similar to that in the conventional waveguide coupler [15]. The period of the optical energy oscillation [e.g., that in Fig. 2(a)] is the least common multiple

[1]Distributed by R-soft Research, Inc.

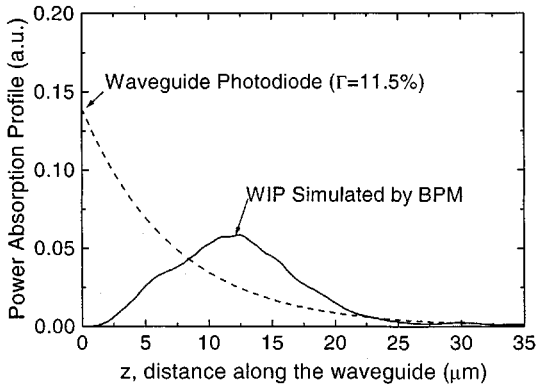

Fig. 3. BPM simulated absorption profile of WIP (solid line) of Fig. 1(a) and the conventional waveguide photodiode (dashed line).

of the effective wavelength of the beating optical modes. Such an efficient coupling is represented by a sharp rise of the effective $\Gamma(z)$ in the absorber, which increases monotonically in the first 20 μm of the absorber. The coupled intensity in the InGaAs is effectively absorbed, in accordance with

$$P(z) = P_0[1 - \exp(-\alpha\Gamma(z)z)] \tag{1}$$

where P_0 is the intensity at the start of the absorber section, z is the distance measured from the same point, and α is the absorption coefficient in the absorber. In the structure without the index-matching layer, the optical intensity is evanescently coupled into the InGaAs layer. The simulated optical intensity profile in the InGaAs and the passive waveguide are shown in Fig. 2(b) (note that the ripple is an artifact of the BPM simulation), which suggests that around 8% of the optical intensity launched into the passive waveguide is coupled into the absorber. Therefore, a waveguide photodiode design employing the evanescent coupling requires a longer absorber region [16].

Next we include the absorption in the InGaAs absorber in the above BPM simulation. The absorption profile along the absorber, which is directly related to the carrier distribution profile, affects the saturation behavior of the waveguide photodiode. The absorption profile along the waveguide $A(z)$ of the WIP in Fig. 1(a) is obtained by taking the spatial derivative of the total optical intensity simulated with the absorption included, and is depicted as the solid line in Fig. 3. In this WIP design, at the absorber front end, where the guided optical intensity is at full strength, a relatively smaller portion of the optical intensity is coupled and absorbed. Away from the absorber front end, the effective Γ increases due to the mode beating, and a larger portion is coupled and absorbed. For comparison, Fig. 3 also depicts the usual exponential decay profile (dashed line) in the ordinary WP or DWP where Γ at the absorber is constant. Thus, the absorption is more spread out along the propagation direction in the WIP.

III. Design Optimization for High Power, High Speed, and High Responsivity

A. High-Power Design

During high-power operation, the performance degradation of a photodiode can show up as catastrophic failure, responsivity reduction at microwave frequency, and nonlinear distortion generation. The distributed absorption of the WIP can raise the critical optical intensity level for these occurrences.

Thermal runaway has been identified as the major mechanism responsible for the catastrophic failure of the photodiode under continuous-wave illumination [17]. The reverse leakage current in photodiodes increases with temperature. As a response to the temperature rise due to the photocurrent heating, more leakage current is generated, which in turn generates more heat. The process repeats and can culminate in device catastrophic failure. The heat generated at the photodiode can be expressed as

$$Q = WD\int_0^L j^2(z)\rho \cdot dz \tag{2}$$

where $j(z)$ is the current density of the photodiode, assumed to be constant across the junction width W, D is the path length along the heat flow, ρ is the series resistivity of the material, z is the propagation distance, and L is the length of the absorption waveguide. Since the current density is proportional to the optical absorption, the absorption profiles shown in Fig. 3 can be used to compare the current distribution profiles of WIP and DWP. According to (2), for the same total photocurrent level, the more well-spread current density profile of WIP is expected to generate less heat than the DWP with the same responsivity and the junction area.

Both the responsivity degradation at microwave frequency and the nonlinear distortion generation can be attributed to the space charge screening effect under high illumination [4], [5]. The screening electric field is opposite in direction to the applied electric field. The net electric field is reduced in magnitude at a portion of the depletion region, and the carrier velocity is reduced at the low field region. Therefore, the responsivity at high frequency is reduced as fewer charges respond to the modulated optical signal [4]. Also, nonlinear distortions are generated due to the following.

1) Carriers have nonuniform transit time.
2) The built-up charge induces nonlinear junction impedance variation in the depletion region [18].

At the absorber, the carrier generation rate per unit length G is the driving force behind the high charge density and is proportional to the absorption $A(z)$

$$G = \frac{A(z)}{h\nu} \cdot \frac{1}{W \cdot d} \tag{3}$$

where W and d are the width and thickness of the absorber layer, respectively. In DWP, the peak absorption is reduced by having a smaller Γ factor at the absorber [6]. However, this may not lower the degree of saturation as the thickness of the absorber d is also reduced in getting the smaller Γ. In contrast, in WIP, the peak absorption can be reduced without reducing d. This is due to the provision of separate optimization of the absorber and the passive waveguide in the WIP design. As a result, a relatively small portion of the optical intensity is coupled to the absorber while the thickness of the absorber can be maximized with respect to the transit time, both of which allow a smaller G to be achievable with the WIP. We have compared the maximum G of the proposed WIP design of Fig. 1 to the DWP with Γ equal

to 11.5% so that both of them have the same absorber length, as shown in Fig. 3. (In that case, the thickness of the InGaAs layer of the DWP can be either 0.11 or 0.15 μm depending on whether the adjacent InGaAsP waveguiding layer is 1.15 or 1.23 μm in λ_g [6].) The ratio of the peak generation rate in WIP to that in DWP then varies from 9.9% to 13.5%. In other words, the maximum carrier generation rate in the proposed WIP design can be reduced to one-tenth of that in the equivalent DWP.

B. High-Speed Design

In general, WIP has two high-speed design advantages over ordinary WPs. For lump-element design, a limiting factor to the RC circuit time is the control of the junction length. The junction length of an ordinary WP is determined by precise mechanical cleavage. In contrast, the junction length of a WIP is defined by the photolithography and the subsequent mesa etching, while cleaving is done at the passive waveguide section. Therefore the junction length of WIP is much better controlled in practice. Also, the width of the absorber of WIP can be tailored for certain microwave impedance values without sacrificing the overall responsivity as the absorber design is decoupled from the waveguide design. This suggests that a high-responsivity *high-power* traveling-wave electrode waveguide photodiode [8], [19], [20] is more readily achievable with the WIP design.

Here, since a lumped element WIP is investigated, we first optimize the dimensions of the absorber subject to the RC time and the carrier transit time limits [21]. As they are oppositely related to the absorber thickness, it may appear that a thin and small absorber can maximize the speed of the photodiode. However, in view of the saturation effect, a large absorption volume is preferred for high-power operation. Therefore, a design strategy is to vary the thickness d, the length L, and the width W of the absorber subject to the maximum absorption volume ($d \times L \times W$) and the minimum bandwidth requirements. The output photocurrent $J(\omega)$ can be expressed as [22]

$$J(\omega) = J_0(\omega) \cdot H(\omega) \tag{4}$$

where $J_0(\omega)$ denotes the frequency response of the photocurrent due to the transit time effect, $H(\omega)$ is the frequency response due to the RC time effect. Ignoring the saturation effect and the diffusion current, $J_0(\omega)$ can be expressed as [22]

$$J_0(\omega) = \frac{qG}{j\omega}\left\{ v_h\left[1 + \frac{v_h}{j\omega d}\left(1 - \exp\left(j\omega\frac{d}{v_h}\right)\right)\right] + v_e\left[1 + \frac{v_e}{j\omega d}\left(1 - \exp\left(j\omega\frac{d}{v_e}\right)\right)\right]\right\} \tag{5}$$

where v_h and v_e are the saturation velocity of the holes and electrons inside the depletion region, respectively. From simple circuit analysis, $H(\omega)$ can be expressed as

$$H(\omega) = \frac{R_J}{(R_S + R_L + R_J) + j\omega\left[(R_S + R_L)R_J C_J\right]} \tag{6}$$

where R_J is the junction resistance, C_J is the junction capacitance, R_s is the series resistance, and R_L is the load resistance. In the calculation, the contact resistivity is assumed to be 2×10^{-5} Ω cm^{-2} and W is set at 3 μm. Fig. 4 plots the 3-dB bandwidth versus L at various ds. From this plot, the absorber layer should be 35 μm long and 0.45 μm thick to provide the maximum absorption volume while still meeting the 50-GHz bandwidth requirement.

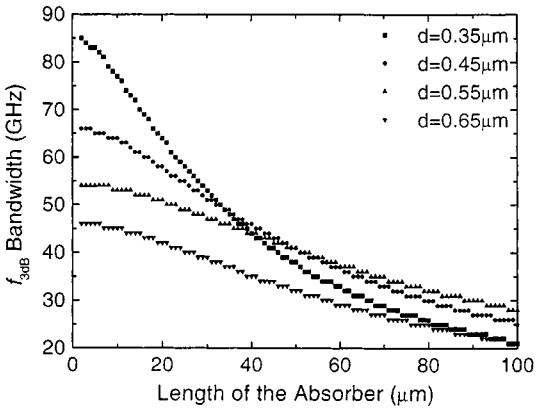

Fig. 4. Calculated 3-dB bandwidth of the lumped element waveguide photodiode as a function of the junction length at different absorber thickness.

C. High-Responsivity Design

The responsivity of the WIP is affected by two separate couplings: between the tapered fiber and the passive waveguide and between the passive waveguide and the absorber. Most prior works focused on improving the coupling between the passive waveguide and the absorber for a given propagation distance [10], [11]. Consequently, the overall responsivity of the WIP can still be limited by the coupling between the tapered fiber and the passive waveguide, especially when a thin passive waveguide is used. In this paper, a ridge waveguide structure with a relatively thick passive waveguide layer ($\sim$1.2 μm) is employed, which corresponds to a simulated 72% coupling efficiency between an antireflection (AR) coated passive waveguide and a tapered fiber with a 3-μm spot size. Making the waveguide even thicker can result in a higher coupling efficiency between the fiber and the waveguide [7]; however, this can also lower the coupling efficiency between the waveguide and the absorber for a given coupling distance. Therefore, we need to examine the appropriate design of the index-matching layer to optimize both couplings.

In our design, the index and the thickness of the index-matching layer are tuned for high responsivity. With BPM simulation, we observe that a high-index matching layer can enhance the coupling efficiency between the passive waveguide and the absorber. However, with an InGaAsP index-matching layer, a high index also implies a smaller bandgap and thus a high residual absorption loss. In our design, the bandgap of the matching layer is chosen to be 1 eV ($\lambda_g = 1.23$ μm) to reduce the residual absorption of 1.32-μm wavelength light. The corresponding index is 3.46 [23]. To minimize the propagation loss, the index of the waveguide layer is chosen to be 3.39 ($\lambda_g = 1.15$ μm). Our simulation results suggest that the WIP with either too thin or too thick a matching layer has a low coupling efficiency between the waveguide and the absorber. For either case, the waveguiding structure quickly approaches that of the evanescent-coupled structure. Based upon the above

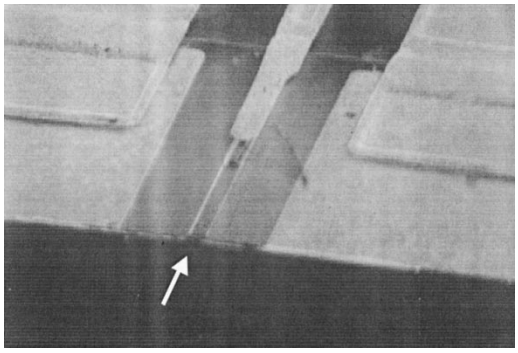

Fig. 5. A SEM top view of the WIP showing the passive waveguide (pointed at by the arrow) and the absorber waveguide covered with metal.

layer structure and index profile, the BPM simulation results indicate that the optimal matching layer thickness is around 0.45 μm for the shortest absorber length.

IV. Device Fabrication

The epitaxial layers shown in Fig. 1(a) are grown by metal-organic chemical vapor deposition on a Fe-doped semi-insulating InP substrate. Using a liftoff technique, the 2.5×35 μm^2 Ti/Pt/Au (150 Å/150 Å/800 Å) p-contact is deposited on top of the p^+-InGaAs layer via e-beam evaporation. The contact is annealed at 460 °C for 30 s. A 35-μm-long absorber mesa is first etched using an etchant consisted of 20 mL of H_2O, 20 mL of HBr, and 20 drops of Br_2. The trapezoidal mesa, as shown in Fig. 1(b), consists of the p^+-InGaAs layer, the p-InP layer, the absorber, and the matching layer. The waveguide is formed by removing 0.6 μm of the passive InGaAsP layer in the second etching step using the same etchant. Ge/Au/Ni/Au (330 Å/600 Å/150 Å/400 Å) n-contacts are deposited on both sides of the etched mesa and are connected to the ground lines of a coplanar waveguide (CPW) transmission line on the semi-insulating substrate. The contact is annealed at 420 °C for 3 min. The center signal line of the CPW is connected to the p-contact via a gold-plated air bridge to minimize the parasitic capacitance [24]. The wafer is then lapped down to $\sim$80 μm thick and is mechanically cleaved into arrays of photodiodes for evaluation. Fig. 5 shows a scanning electron micrograph (SEM) of the finished WIP.

V. Measurement Results and Discussion

The dc characteristics of the photodiode are measured by a semiconductor parameter analyzer (HP4145B). The typical dark current is less than $<$10 nA at -6 V and reaches 1 μA at -15 V for a device without any mesa sidewall passivation. The series resistance is $\sim$20 Ω when the forward-bias current is 10 mA.

The microwave responsivity of the WIP is measured using a lightwave vector network analyzer (HP8703A). The microwave loss of the cable, the bias tee, and the microwave probe (Cascade ACP) are calibrated out using a full two-port calibration with a standard impedance substrate (Cascade LRM ISS GSG). The modulated optical power from the HP8703A is at 1.3 μm wavelength. It is coupled to the WIP through a single-mode tapered fiber with a spot radius about $1.75 \sim 2.25$ μm. The microwave responsivity of the WIP from 200 MHz to 20 GHz is

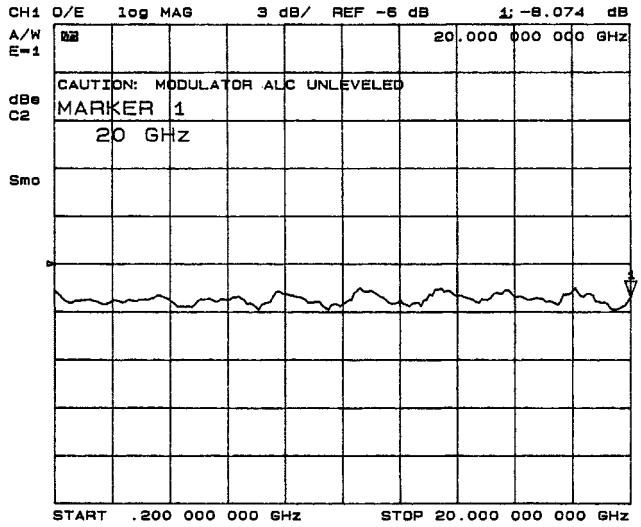

Fig. 6. The frequency response of the WIP measured by HP 8703A. The responsivity at 20 GHz is about 0.40 A/W. The device is biased at -6 V, and the photocurrent is 120 μA.

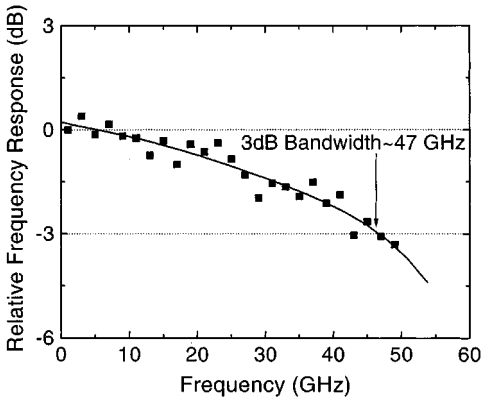

Fig. 7. Frequency response of the WIP using heterodyned laser setup. The 3-dB bandwidth of the WIP is $\sim$47 GHz. The device is biased at -9 V and the photocurrent is 84 μA.

plotted in Fig. 6, with the device biased at -9 V bias and at 120 μA dc photocurrent. Without AR coating, the device exhibits a responsivity of 0.4 A/W at 20 GHz. The responsivity variation remains within $\pm$0.6 dB at different optical polarization.

While the above measurement shows that the small signal responsivity of the WIP is flat up to 20 GHz, the setup is not capable of measuring the 3-dB frequency of the device that is well beyond 20 GHz. Therefore, we use another setup with two lasers optically heterodyned to generate an RF tone up to 50 GHz [24]. The two temperature-tuned Nd : YAG lasers have similar optical power and polarization and emit at $\sim$1.318 μm wavelength. The output microwave signal of the WIP is measured by a high-frequency microwave power meter (HP 437B). The microwave loss of the microwave probe, the cable, and the bias tee is calibrated out using a method proposed in [26]. The characteristic impedance of the microwave probe (Cascade ACP) and the rest of the system are 50 Ω. With the WIP biased at -9 V and at 100 μA dc photocurrent, the measured 3-dB rolloff frequency is 47 GHz, as depicted in Fig. 7, which is close to the designed value.

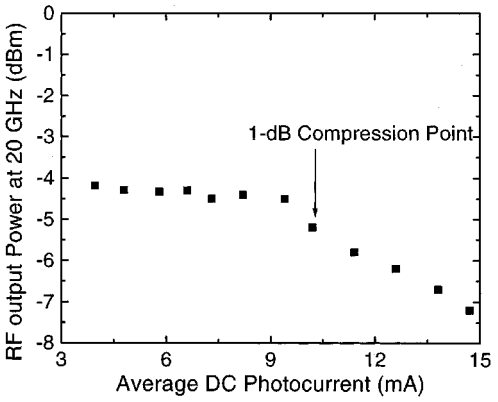

Fig. 8. The measured RF output of WIP at 20 GHz at a function of the dc photocurrent. The device is biased at −6 V.

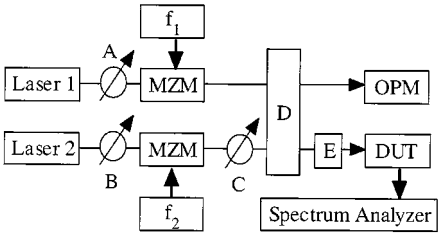

Fig. 9. Two-tone setup for measuring the IP3 of the photodiode. A, B, and C are polarization rotators; D is a 3-dB coupler; E is an optical attenuator; OPM stands for optical power meter; and DUT is device under test. The microwave sources contain an isolator and a bandpass filter.

For analog fiber-optics link, the degradation of the microwave responsivity under high optical power is one of the main concerns for the overall link gain. To characterize the responsivity degradation at high power, the microwave output of the WIP is measured as the average incident optical power is varied. As in the measurement above, the optical RF tone is generated using two temperature-tuned Nd : YAG lasers, whose output is combined with that from a 1.55-μm wavelength laser using a polarization-insensitive WDM coupler, and then coupled to the WIP. The heterodyned signal generates a constant RF tone at the WIP, while the 1.55-μm laser is attenuated to vary the dc optical power. In Fig. 8, the microwave output of the WIP at 20 GHz is plotted against dc photocurrent with the device biased at −6 V. The 1-dB compression point of the output microwave power occurs at 10.2-mA photocurrent.

For analog fiber-optic link, the nonlinear distortions of the photodiode can affect the link SFDR [27]. Among the nonlinear distortions, the two-tone third-order intermodulation distortions (IMD3s) attract particular attention as their frequencies are close to the fundamental signals. Consequently, a two-tone measurement is carried out to extract the output referenced third-order intercept point (IP3) of the WIP. The measurement setup is similar in concept to that in [28]. The tones f_1 and f_2 are separately generated in the two links, each consisting of an Nd : YAG laser and a Mach–Zehnder modulator (MZM) driven by a microwave synthesizer, as shown in Fig. 9. A 3-dB optical coupler is used to combine the two modulated optical signals. In our approach, by biasing the MZM at the quadrature point to minimize the second harmonic distortions (HD2), the second-order intermodulation distortions at $2f_1$-f_2 and $2f_2$-f_1 arising from the second harmonic of one tone and the fundamental of the other tone can be minimized. Therefore, the IMD3 at the photodiode can be more accurately measured. This, together with appropriate microwave isolators and bandpass filters between the microwave synthesizers and the modulators, results in a larger than 50 dB suppression of the HD2. The extra spurious signals due to the beating of the two free-running Nd : YAG lasers can be minimized by keeping the two beams orthogonal polarized. A spectrum analyzer is used to measure the fundamental and the IMD3 signals at the photodiode output at different input microwave powers. Fig. 10 shows the measurement results with f_1 and f_2 set at 1 and 1.04 GHz, as well as 18 and 18.04 GHz at −9 V bias. The output referenced IP3 is extrapolated from the fundamental and the IMD3. The IP3 reaches +20.32 dBm at 1 GHz and +5.35 dBm at 18 GHz at 1.85 mA photocurrent. The SFDR of the shot-noise limited fiber-optic link using this WIP is estimated at 124 dB/Hz$^{2/3}$ at 1 GHz and 114 dB/Hz$^{2/3}$ at 18 GHz when a linearized modulator is used at the transmitter [29].

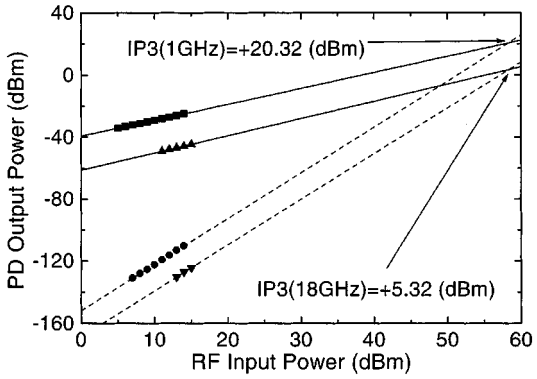

Fig. 10. Measured fundamental (■) and IMD3 (•) signals at 1 GHz, and measured fundamental (▲) and IMD3 (▼) at 18 GHz versus input RF signals, with 1.85 mA photocurrent and −9 V bias.

VI. Conclusion

In summary, we have designed, fabricated, and evaluated a WIP that employs an index-matching layer and a thick passive waveguide layer for high saturation current, high speed, and high responsivity purposes. For photodiodes fabricated so far using this WIP design, the 1-dB RF output power compression point at 20 GHz occurs at 10.2 mA photocurrent; the RF responsivity at 20 GHz is 0.4 A/W without AR coating; and the output referenced IP3 is +20.32 dBm at 1 GHz and +5.35 dBm at 18 GHz for 1.85 mA photocurrent. The 47-GHz 3-dB bandwidth measured is consistent with the design of the absorber. This WIP can meet the high SFDR requirement of analog fiber links.

Acknowledgment

The authors are indebted to Dr. T. A. Vang at TRW for his encouragement and support of this work. They would also like to acknowledge J. Lacey and D. Forbes at TRW for the epitaxial growth; and G. L. Li, D. S. Shin, Prof. Y. Fainman, and Prof. B. Rickett at the University of California at San Diego for their

helpful discussions. The authors would like especially to thank Dr. S. A. Pappert for the loan of the Nd : YAG lasers and modulators.

REFERENCES

[1] G. E. Betts, L. M. Johnson, and C. H. Cox III, "Optimization of externally modulated analog optical links," in *Proc. SPIE.*, vol. 1562, 1991, pp. 281–302.

[2] K. J. Williams, L. T. Nichols, and R. D. Esman, "Photodetector nonlinearity limitations on a high-dynamic range 3 GHz fiber optic link," *J. Lightwave Technol.*, vol. 16, pp. 192–199, 1998.

[3] K. Kato, "Ultrawide-band/high-frequency photodetectors," *IEEE Trans. Microwave Theory Tech.*, vol. 47, pp. 1265–1281, 1999.

[4] A. R. Williams, A. L. Kellner, and P. K. L. Yu, "High frequency saturation measurements of an InGaAs/InP waveguide photodetector," *Electron. Lett.*, vol. 29, pp. 1298–1299, 1993.

[5] J. Harari, G. Jin, J. P. Vilcot, and D. Decoster, "Theoretical study of p-i-n photodetectors' power limitations from 2.5 to 60 GHz," *IEEE Trans. Microwave Theory Tech.*, vol. 45, pp. 1332–1336, 1997.

[6] H. Jiang, J. T. Zhu, A. L. Kellner, and P. K. L. Yu, "High-saturation-power waveguide photodetector for analog fiber-optic links," in *Proc. SPIE.*, vol. 2844, 1996, pp. 120–124.

[7] K. Kato, S. Hata, A. Kozen, J. Yoshida, and K. Kawano, "Highly efficient 40 GHz waveguide InGaAs p-i-n photodiode employing multimode waveguide structure," *IEEE Photon. Technol. Lett.*, vol. 3, pp. 820–822, 1991.

[8] L. Y. Lin, M. C. Wu, T. Itoh, T. A. Vang, R. E. Muller, D. L. Sivco, and A. Y. Cho, "High-power high-speed photodetectors design, analysis and experimental demonstration," *IEEE Trans. Microwave Theory Tech.*, vol. 45, pp. 1310–1319, 1997.

[9] S. Jasmin, N. Vodjdani, J. C. Renaud, and A. Enard, "Diluted and distributed absorption microwave waveguide photodiodes for high efficiency and high power," *IEEE Trans. Microwave Theory Tech.*, vol. 45, pp. 1337–1341, 1997.

[10] L. Giraudet, F. Banfi, S. Demiguel, and G. Herve-Gruyer, "Optical design of evanescently coupled, waveguide-fed photodiodes for ultrawide-band applications," *IEEE Photon. Technol. Lett.*, vol. 11, pp. 111–113, 1999.

[11] A. Umbach, D. Trommer, G. G. Mekonnen, W. Ebert, and G. Unterborsh, "Waveguide integrated 1.55 μm photodetector with 45 GHz bandwidth," *Electron. Lett.*, vol. 32, pp. 2143–2144, 1996.

[12] J. F. Vinchant, F. Mallecot, D. Decoster, and J. P. Vilcot, "Effects of absorbing layers on the propagation constant: a four layer model on desktop-computer applied to photodetectors monolithically integrated with optical waveguides," *Opt. Commun.*, vol. 76, pp. 266–270, 1988.

[13] R. J. Hawkins, R. J. Deri, and O. Wada, "Optical power transfer in vertically integrated impedance-matching waveguide/photodetectors: physics and implications for diode length reduction," *Opt. Lett.*, vol. 16, pp. 470–472, 1991.

[14] R. J. Deri and O. Wada, "Impedance matching for enhanced waveguide/photodetector integration," *Appl. Phys. Lett.*, vol. 55, pp. 2712–2714, 1989.

[15] D. Marcuse, "Directional couplers made of nonidentical asymmetric slabs. Part I: Synchronous couplers," *J. Lightwave Technol.*, vol. LT-5, pp. 113–118, 1987.

[16] S. Chandrasekhar, J. C. Campbell, A. G. Dentai, and G. J. Qua, "Monolithic integrated waveguide photodetector," *Electron. Lett.*, vol. 23, pp. 501–502, 1987.

[17] J. S. Paslaski, P. C. Chen, J. S. Chen, C. M. Gee, and N. Bar-Chaim, "High-power microwave photodiode for improve performance of RF fiber optic links," in *Proc. SPIE*, vol. 2844, 1996, pp. 110–119.

[18] H. Jiang and P. K. L. Yu, "Equivalent circuit analysis of harmonic distortions in photodiode," *IEEE Photon. Technol. Lett.*, vol. 10, pp. 1608–1610, 1998.

[19] V. M. Hieala, G. A. Vawter, T. M. Brennan, and B. E. Hammons, "Traveling-wave photodetectors for high-power, large bandwidth applications," *IEEE Trans. Microwave Theory Tech.*, vol. 43, pp. 2291–2297, 1995.

[20] K. Giloney, M. J. Rodwell, and J. Bowers, "Traveling-wave photodetector theory," *IEEE Trans. Microwave Theory Tech.*, vol. 45, pp. 1320–1331, 1997.

[21] J. Bowers and C. Burrus, "Ultrawide-band long-wavelength p-i-n photodetectors," *J. Lightwave Technol.*, vol. LT-5, pp. 1339–1350, 1987.

[22] P. Bhattacharya, *Semiconductor Optoelectronic Devices*. Englewood Cliffs, NJ: Prentice-Hall, 1994, p. 350.

[23] B. Reid, R. Macieiko, and A. Champagne, "Absorption and index of refraction for the modeling of InGaAsP/InP photonic devices," *Can. J. Phys.*, vol. 71, pp. 410–416, 1993.

[24] A. R. Williams, A. L. Kellner, X. S. Jiang, and P. K. L. Yu, "InGaAs/InP waveguide photodetector with high saturation intensity," *Electron. Lett.*, vol. 28, pp. 2258–2259, 1992.

[25] D. J. Mcquate, K. W. Chang, and C. J. Madden, "Calibration of lightwave detectors to 50 GHz," *Hewlett-Packard J.*, pp. 87–92, 1993.

[26] P. Debie, L. Martens, and D. Kaiser, "Improved error correction technique for on-wafer lightwave measurement of photodetectors," *IEEE Photon. Technol. Lett.*, vol. 7, pp. 418–420, 1995.

[27] T. A. Vang, D. C. Scott, L. J. Lembo, J. Elliott, D. Forbes, K. Everett, R. Johnson, J. Lacey, A. Krispin, F. Alvarez, E. T. Kunkee, and J. Brock, "High power, high frequency waveguide photodetectors," in *Proc. LEOS Annu. Meeting*, San Francisco, CA, Nov. 8–11, 1999, pp. 804–805.

[28] T. Ozeki and E. H. Hara, "Measurement of nonlinear distortion in photodiodes," *Electron. Lett.*, vol. 12, no. 3, pp. 80–81, 1976.

[29] J. A. Schaffner and W. B. Bridges, "Intermodulation distortion in high dynamic range microwave fiber-optic links with linearized modulators," *J. Lightwave Technol.*, vol. 11, pp. 3–6, 1993.

Hao Jiang received the B.S. degree in materials science from Tsinghua University, China, in 1994 and the Ph.D. degree in electrical engineering from the University of California, San Diego, in 2000.

He is currently a Device Engineer with Conexant Systems Inc., Newport Beach, CA, and participates in the development of CMOS imagers.

Paul K. L. Yu (M'84–SM'90) received the Ph.D. degree in applied physics from the California Institute of Technology, Pasadena, in 1983.

In 1983, he joined the Faculty of the Department of Electrical and Computer Engineering, University of California at San Diego, where he has been a Professor since 1993. His research interests include materials and device for fiber optics and microwave photonics applications.